NASA-TP-2304 19840016510

NASA Technical Paper 2304

May 1984

Lewis Research Center Spin Rig and Its Use in Vibration Analysis of Rotating Systems

Gerald V. Brown,
Robert E. Kielb,
Erwin H. Meyn,
Richard E. Morris,
and Stephen J. Posta

NASA

NASA
Technical
Paper
2304

1984

Lewis Research Center Spin Rig and Its Use in Vibration Analysis of Rotating Systems

Gerald V. Brown,
Robert E. Kielb,
Erwin H. Meyn,
Richard E. Morris,
and Stephen J. Posta

Lewis Research Center
Cleveland, Ohio

National Aeronautics
and Space Administration

Scientific and Technical
Information Branch

Summary

The Lewis Research Center spin rig was constructed to provide experimental evaluation of analysis methods developed under the NASA Engine Structural Dynamics Program. Rotors up to 51 cm (20 in.) in diameter can be spun to 16 000 rpm in vacuum by an air motor. Vibration forcing functions are provided by shakers that apply oscillatory axial forces or transverse moments to the shaft, by a natural whirling of the shaft, and by an air jet. Blade vibration is detected by strain gages and optical tip blade-motion sensors. A variety of analog and digital processing equipment is used to display and analyze the signals.

Results obtained from two rotors are discussed. A 56-blade compressor disk was used to check proper operation of the entire spin rig system. A special two-blade rotor was designed and used to hold flat and twisted plates of various setting and sweep angles. Accurate Southwell coefficients have been obtained for several modes of a flat plate oriented parallel to the plane of rotation.

Introduction

The Lewis Research Center spin rig provides experimental evaluation of vibration analysis methods for rotating systems. Bladed rotors up to 51 cm (20 in.) in diameter can be spun to 16 000 rpm by a speed-regulated air motor. Electromagnetic shakers apply oscillatory axial forces or transverse moments to the rotor shaft through a thrust bearing. A slight natural rotor whirl and an air jet provide additional "engine-order-dependent" forcing functions. Strain gages and optical blade-tip vibration sensors provide blade vibration signals. Results from two rotors have demonstrated the strengths of the rig and suggest additional improvements. A two-blade rotor, on which the blade setting and sweep angles can be adjusted, has yielded high-precision resonant frequencies for a dozen or more bending, torsion, and plate modes. Very sharp resonances have been obtained for the first several resonant frequencies, and this has led to very precise Southwell coefficients against which to check theoretical predictions. In a mid-span-shrouded compressor assembly with a relatively stiff disk, system modes with zero and one nodal diameter of the first bending family can be produced, as can some modes in the first torsion family. No observable second bending mode nor pure system modes with more than one nodal diameter have been produced. Modes produced by the air jet likely include modes with more than one nodal diameter, but the decomposition of the motion into pure modes has not yet been attempted. The fuller use of the optical system and decomposition of the more complex observed vibrations are expected to permit measurement precision approaching that obtained on the two-blade rotor to be obtained on multiblade rotors.

In this report the physical characteristics of the rig are discussed and the available instrumentation is described. Then calculated vibration characteristics and experimental results for a 56-blade rotor are presented in several sections. Finally the first results obtained from an adjustable two-blade rotor are presented.

Physical Characteristics of the Spin Rig

Figure 1 is a cutaway drawing of the rig showing the vacuum tank, the air motor drive, two electromagnetic shakers, a multiblade rotor, a 100-channel slipring assembly, and an indication of the optical probe system for blade-tip observation. The vacuum (less than 1 torr) reduces the torque required to drive the disk and renders aerodynamic effects negligible. The air motor can spin a disk such as the one shown in the figure to 16 000 rpm in about 3 min and contains an air brake that can stop the disk from that speed in about 18 min. Faster shutdown can be achieved by admitting air to the tank.

The two 220-N (50-lbf) shakers move the shaft by acting on the outer race of a thrust bearing. Shaft motion is permitted because the rotor bearings are mounted on rubber supports. These supports introduce damping into all modes that couple to axial or transverse motion of the shaft. The shakers can also be operated out of phase. This applies a slight oscillatory moment to the upper part of the shaft and is more effective for producing some blade vibration modes than is pure axial motion.

Figure 2 presents oscilloscope traces of the transverse orbits at locations near each bearing of the rotor shaft. The traces were obtained from proximity probes mounted 90° apart at each location, with no shaker

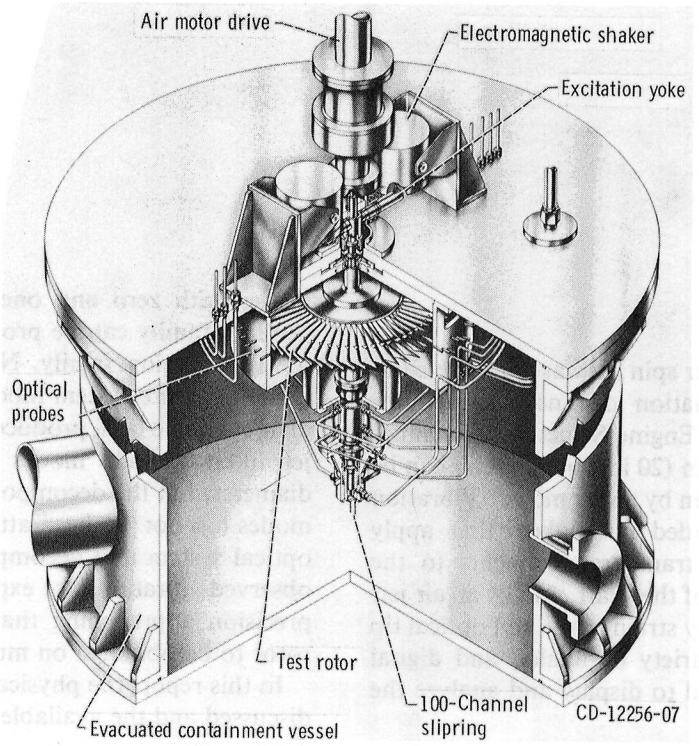

Figure 1. – Cutaway drawing of spin rig.

excitation. The deflections in the two perpendicular directions are plotted in figure 3 as functions of rotational speed. This transverse motion aids in producing one-nodal-diameter modes in a multiblade rotor as well as modes with any component of motion in the plane of rotation. It is not, of course, controllable.

At the bottom of the rotor is a 100-channel slipring assembly for strain-gage leads. The assembly is cooled and lubricated by a mixture of oil and chlorofluorocarbon. A seal system prevents loss of the fluid into the evacuated rig.

A simple air jet, issuing from a 1.65-mm-i.d. tube, can be directed at the blades to excite engine-order modes (modes which have frequencies that are integer multiples of the rotational frequency and nodes that are fixed in space). Figure 4 shows strain-gage signals from five blades on the 56-blade rotor running at low speed (approx 800 rpm) in air. Each blade receives an impulse from the jet and then undergoes damped oscillation until the next impulse occurs. At this speed the shrouds are not firmly locked. In a later section higher speed results are discussed.

Instrumentation

With the exception of the controlling and monitoring equipment necessary to operate the rig, the instrumentation falls into two categories—that used to obtain the forcing functions and that used to monitor the response. As mentioned previously the forcing functions are obtained from proximity probes that measure axial and transverse displacement of the shaft. The response monitoring systems obtain their data from strain gages and optical probes. Signals from the strain-gage conditioners are amplified by a factor of about 2000 and can be displayed on oscilloscopes or oscillographs, recorded in groups of 14 on tape, analyzed by a four-channel fast Fourier analyzer, or displayed in root-mean-square form by processing through rms meters. On the 56-blade rotor that has been used to explore the rig capabilities, three strain gages are mounted on every other blade. The gage placements are shown in figure 5. The A gage is mounted at a 45° angle to the elastic axis of the blade in order to be sensitive to torsional deformation. The B gage is placed to be sensitive to bending deformation. The C gage is placed on the shroud to be sensitive to any modes with significant strains in the shroud.

An optical probe for observing blade-tip deflection is shown in figure 6. Groups of three such probes are mounted on the housing at a number of circumferential locations, as shown in figure 7. The use of three probes at each location allows bending, torsion, and chordwise-bending modes to be distinguished. Each probe contains a light-emitting diode and a light-sensing diode. The

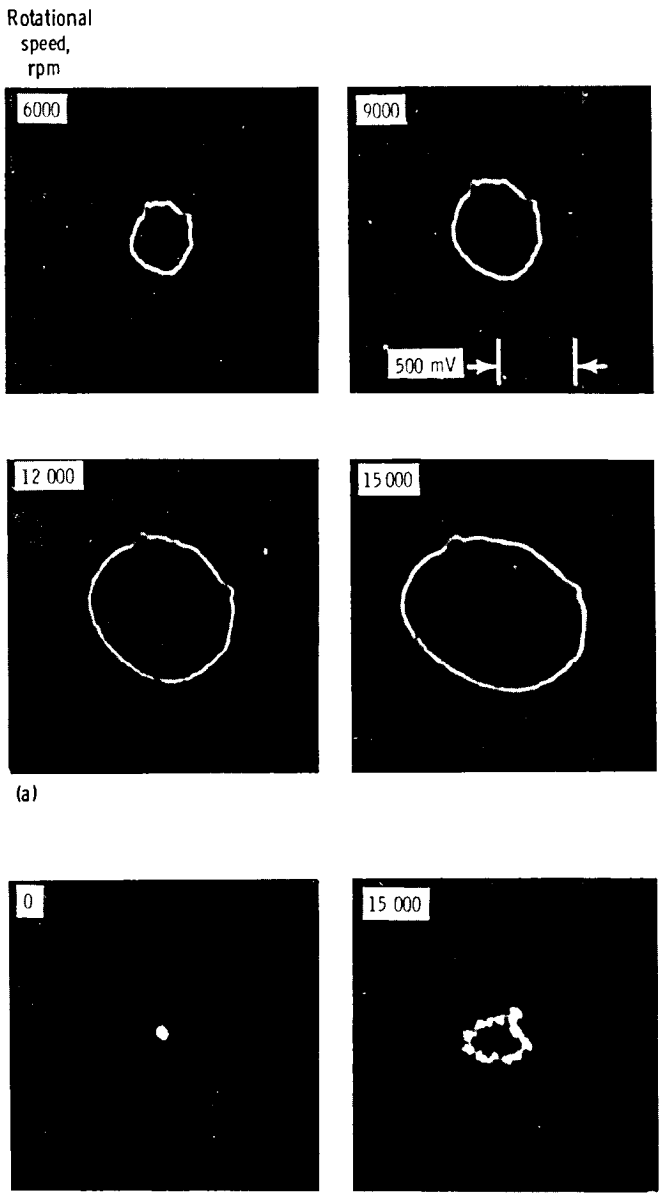

(a) Lower bearing.
(b) Upper bearing.

Figure 2. – Shaft orbits at two locations as functions of rotor speed. (Proximity probe output is 400 mV/0.001 in. Major oscilloscope division equals 500 mV.)

latter produces a signal when light from the former is reflected from a passing blade tip. Circuits mounted behind the emitter-sensor unit sharpen the pulse to permit more precise time measurement. A computing system (ref. 1) compares the blade passage time to the time expected for a nonvibrating blade in order to yield the blade deflection. The expected sensitivity of the measuring system is also discussed in reference 1. The system became fully operational just before this report was completed.

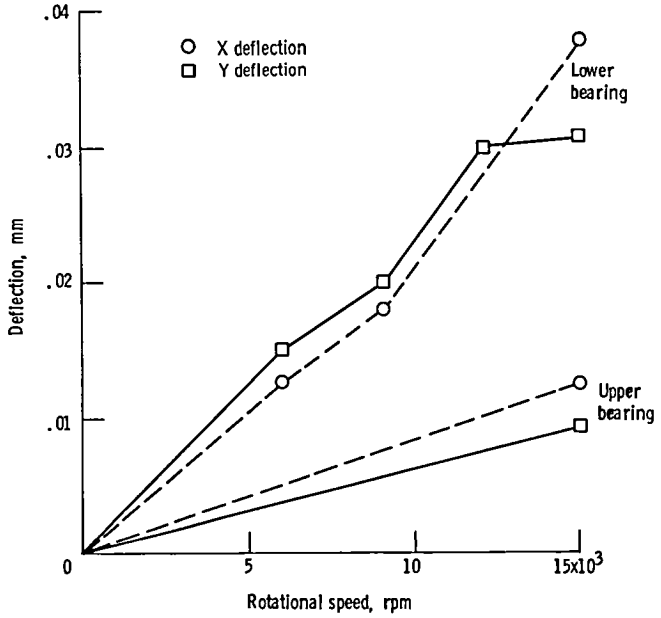

Figure 3. – Transverse bearing displacements as functions of rotational speed (rotor 12).

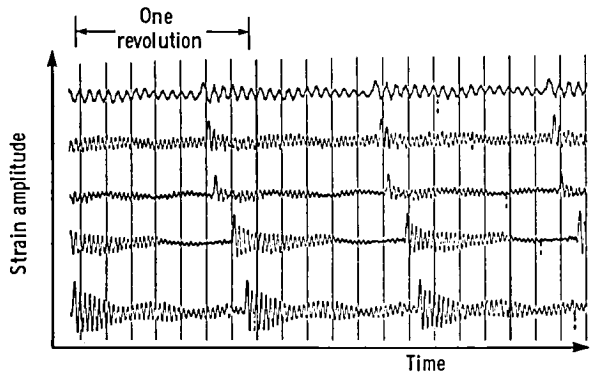

Figure 4. – Blade vibration excited by air jet at low rotational speed (approx 8000 rpm).

Calculated Results for a 56-Blade Rotor (Rotor 12)

The first rotor used to explore the capability of the rig is pictured in figure 8. It is a compressor stage designed for aerodynamic performance tests (ref. 2) and has mid-span shrouds and a relatively stiff disk. This rotor was too stiff and too complicated to serve as an ideal learning tool, but some interesting results were nevertheless obtained.

Bench tests of a shrouded rotor are, of course, somewhat difficult because the shrouds must be artificially locked if system modes are to be obtained or, in fact, to get meaningful data on individual blades. Furthermore appropriate tests to get static single-blade frequencies that would aid in analyzing rotating results are difficult to design. For example, the presence or absence of mistuning depends to a considerable extent in the spinning rotor on the nature of the contact between

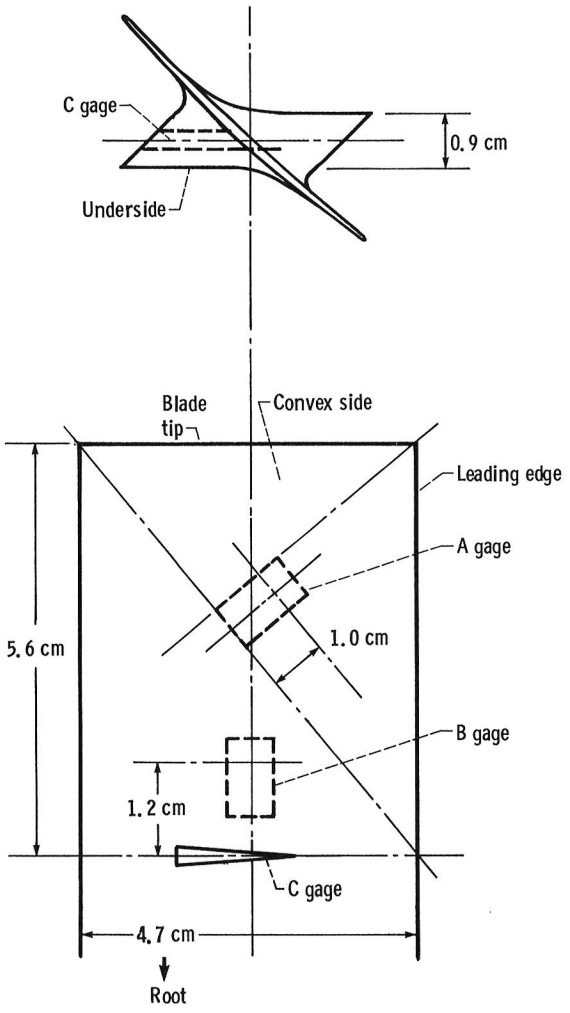

Figure 5.—Strain-gage locations on rotor 12 blade. (Dimensions are in centimeters.)

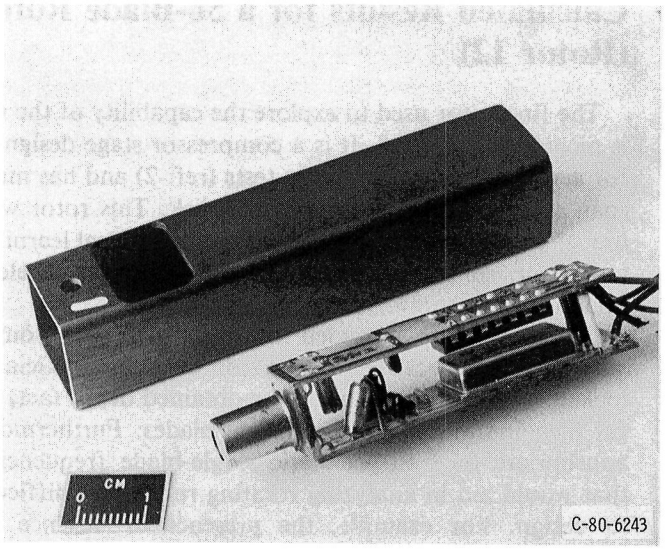

Figure 6. – Optical blade-tip-observation probe, showing sensor, pulse-sharpening circuity, and case.

adjacent shrouds and hence varies with rotational speed. Individual blade data were not available before the rotor was mounted in the rig, but some holograms of system modes were obtained by shimming the shrouds. The resulting mode frequencies did not correlate well with modes observed in the spin rig.

In the absence of adequate bench data and to provide predicted frequencies as a function of rotational speed, a finite-element model of one of the rotor blades was constructed. NASTRAN was used to predict individual blade resonant frequencies and, by using the cyclic symmetry capability of NASTRAN (modified to account for differential stiffness), to predict the frequencies of the assembled bladed disk. Triangular plate elements were used to model the airfoil and neck (64 elements) and the shroud (8 elements). The platform was omitted. The blade was assumed to be cantilevered. Since the proper boundary condition at the shroud contact between adjacent blades is not known, three limiting cases were considered. The first two cases were simple free and fixed boundary conditions. In both of these cases the blades are uncoupled and cyclic symmetry is not needed. The resonant frequencies for these two cases are plotted in figure 9 in the absence of rotation. The fixed shroud constraint gives much higher frequencies than for the free case. For the third case the intrashroud loads are assumed to be so high that continuity of displacement and slope is maintained across the shroud interface. In other words the shrouds act as a continuous ring connected to the blades. It is expected that this condition is approached at the higher speeds. Under this assumption the cyclic symmetry option of COSMIC NASTRAN was used to calculate static and rotating natural frequencies, from which the Southwell coefficient was obtained for harmonic indices of 0, 1, 2, 3, and 28. (The Southwell coefficient is defined in the section Two-Blade Rotor Tests.) From the predicted nonrotating frequencies for this case and the Southwell centrifugal stiffening formula, the additional frequencies needed to construct the plots were calculated for the rotating case. Each single-blade mode becomes a family of modes in the 56-blade rotor, and the members of the family can be enumerated by the number of nodal diameters in the system mode. These families are plotted in figure 9. The mode shapes for one blade in the system mode with no nodal diameters are shown in figure 10 for the first and second bending and first torsion modes.

For the first bending family the frequency increases monotonically with the number of nodal diameters. A blade with free shrouds has a lower first bending frequency, and one with fixed shrouds a higher first bending frequency, at all rotational speeds, than does any mode of the interacting rotor. In the 28-nodal-diameter mode, however, there is a node between each pair of adjacent blades with little motion but considerable stress in the shrouds, so that the frequency of that system mode is

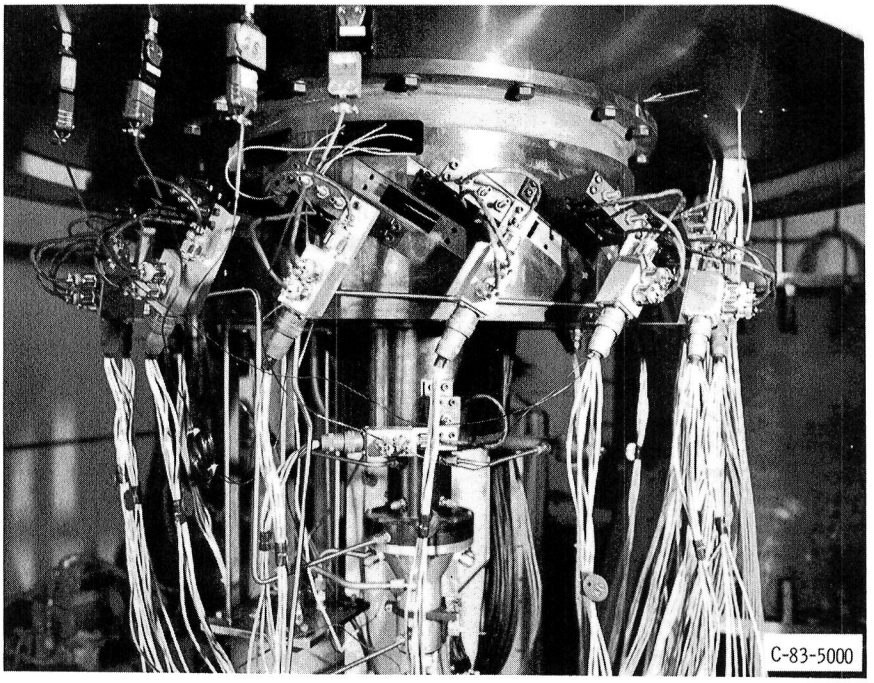

Figure 7. – Array of optical probes mounted in rig.

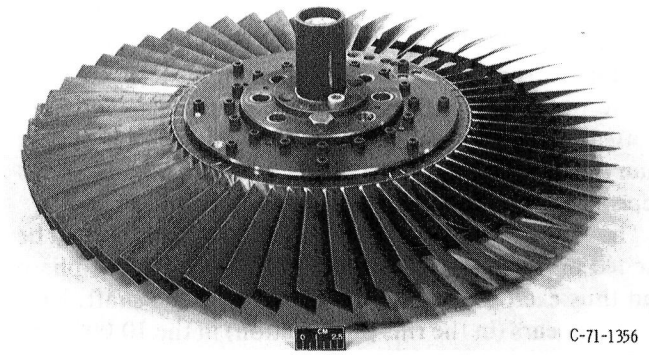

Figure 8. – Rotor 12.

only slightly lower than for the fixed-shroud case. The effect of the centrifugal field (centrifugal stiffening) is fairly strong in the first bending family and at 16 000 rpm increases the frequency of the mode with zero nodal diameters by about 210 Hz above the 410 Hz of the nonrotating case.

The first torsion family is a very closely spaced group of modes with only modest centrifugal stiffening effects. At 16 000 rpm the frequencies are only about 10 percent higher than at zero speed. It is interesting that in this family the mode with zero nodal diameters is not the lowest frequency mode at any speed; several modes lie lower. These lower modes are those with 1, 3, and 28 nodal diameters. It is not hard to believe that the mode with 28 nodal diameters would have a lower frequency than that with no nodes, because in the mode with 28 nodal diameters, adjacent blades are 180° out of phase and the shroud, if firmly locked, is in a simple bending shape. On the other hand, if all blades vibrate in phase, the shroud segment between each pair of blades must strain into an s-like shape, which apparently would involve more strain energy. Whether other modes than those with 1, 3, and 28 nodes lie lower than the zero-nodal-diameter mode has not been investigated.

The second bending family is widely spaced with the 28-nodal-diameter mode having a frequency nearly three times that of the zero-nodal-diameter modes. This behavior is a result of the shroud being at a radial location that is approximately at the antinode of the blade-alone second bending mode (fig. 10).

Experimental Results for Rotor 12

One way to search for observable modes in the rig is to record the root-mean-square average signals (the so-called heating value) from the strain gages as a function of shaker frequency. Such a record is shown in figure 11 where the rotational speed was held constant while the shaker frequency was slowly ramped. One characteristic of this kind of record is that the same blade resonance (i.e., the same blade frequency) often appears more than once. For example, in the torsion gage record of figure 11, a group of three resonance peaks (indicated by arrows) occurs at each speed. The blade is found to be vibrating at the same frequency in all three peaks. The central peak is excited when the frequency of the axial shaker equals the blade resonant frequency; the left peak is excited when the shaker frequency plus the rotating frequency equals the blade frequency; the right peak is

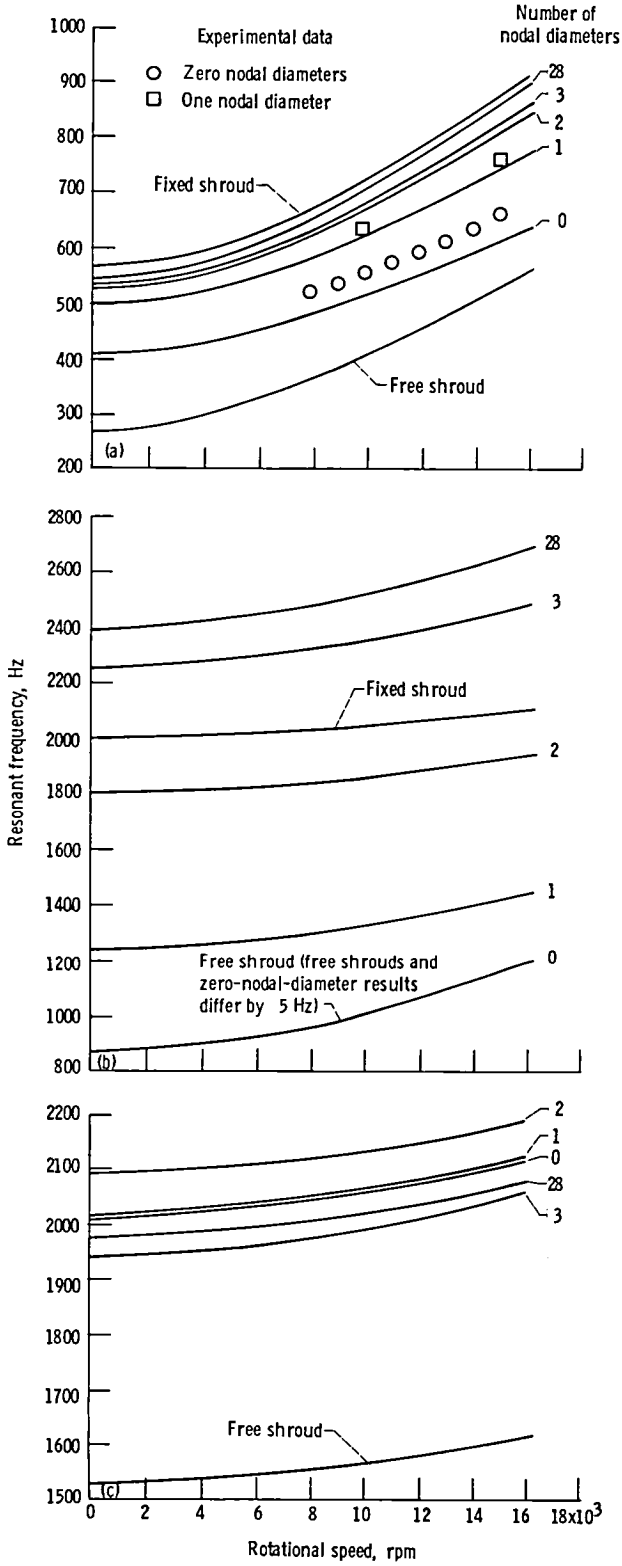

(a) First bending family.
(b) Second bending family.
(c) First torsion family.

Figure 9. – Campbell diagrams for rotor 12.

excited when the shaker frequency minus the rotating frequency equals the resonant frequency. That the blade vibrates at the same frequency in each of the three peaks was verified by counting the frequency of the strain-gage signals directly or by using a modal analyzer on the signals.

The mode that is most strongly excited in the rig is, as expected, the first bending mode with no nodal diameters—the so-called umbrella mode. All the blades vibrate in phase as shown by the raw strain-gage signals reproduced in figure 12. The mode is more clearly and ideally excited at high speeds because the rigidity and continuity of the shroud ring improve as the centrifugal field untwists the blades and causes firmer contact between adjacent shroud segments. This lockup phenomenon is shown clearly in figure 13, a series of rms records from eight strain gages mounted on the shroud segments of every fourth blade in one section of the rotor. In the lower speed records some gages are completely inactive, an indication that the shroud segments are in such loose contact that no observable strain arises. At 10 000 rpm all traces are active, and the sharp resonance peak that appears in each trace is the umbrella mode, which occurs at 552 Hz at that speed. At lower speeds those first bending peaks that do occur are both weaker and broader, probably because of frictional damping at shroud interfaces that are not in firm contact.

The observed frequencies for the umbrella mode are plotted in figure 9(a). Because they lie uniformly higher than those predicted by the NASTRAN model, the model appears to be slightly less stiff than it should be.

The first bending mode with one nodal diameter can be excited in this disk if the shakers are driven out of phase and thus exert an oscillatory moment on the shaft. This mode appears (in the rms presentation) in the 10 000-rpm record of figure 13 at about 80 Hz above the umbrella mode. Raw strain-gage signals for the mode are shown in figure 14. The node lies somewhere between blade 11 and blade 15; the signals on the two sides of the node are 180° out of phase with each other. The node rotates with the disk. The one-nodal-diameter first bending mode also occurs at 15 000 rpm without shaker excitation, apparently because the slight whirling of the shaft (spinning at 250 Hz) excites the one-nodal-diameter mode at three times that frequency.

Because under many conditions two or more modes are excited simultaneously, interpretation is difficult. However, one such superposition is very clear. At 15 000 rpm the one-nodal-diameter first bending mode occurs spontaneously at 750 Hz as just noted. If the shakers are operated in phase at 651 Hz to excite the umbrella mode, both modes occur together. They beat at the difference frequency of 99 Hz as shown in figure 15. Note that the node for the one-nodal-diameter mode occurs near the third trace from the top. The beats on the upper traces have maxima that are out of phase with the maxima on

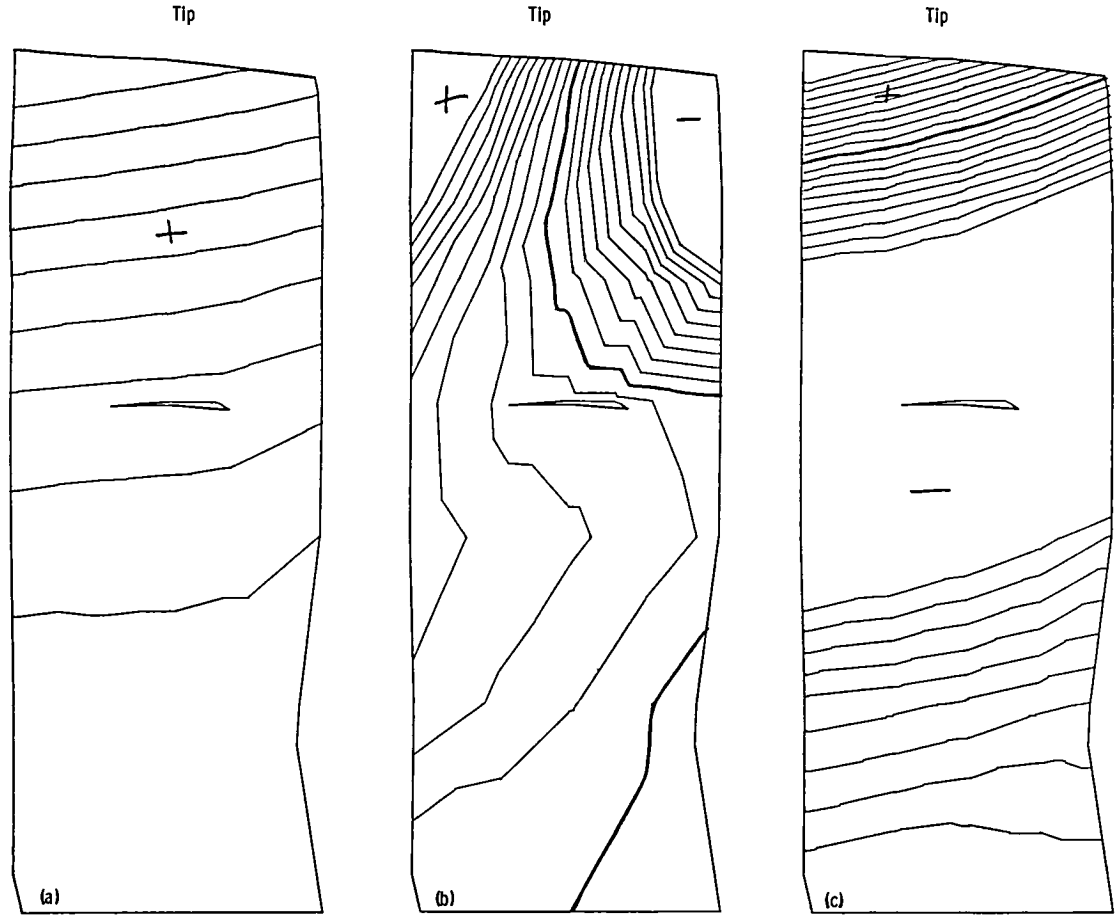

(a) First bending mode (268 Hz). (b) First torsion mode (869 Hz). (c) Second bending mode (1529 Hz).

Figure 10. – Calculated mode shapes for blade in rotor 12, with continuous shrouds in system mode with zero nodal diameter.

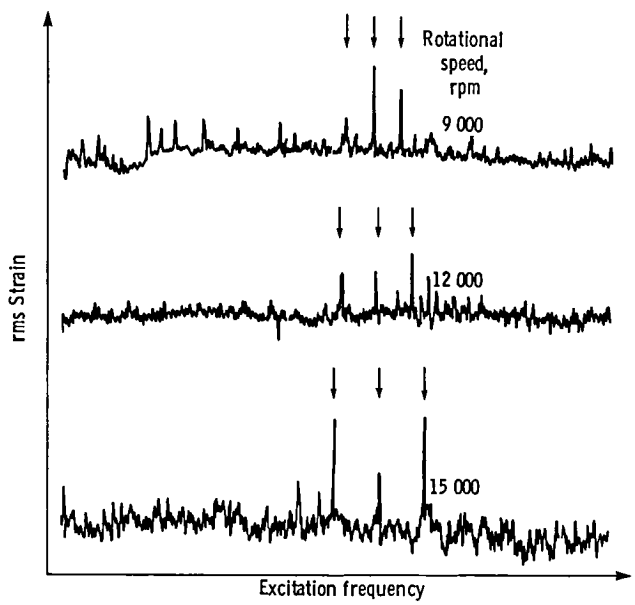

Figure 11. – Root-mean-square presentation of strain-gage signals as functions of shaker frequency. Torsion gage on blade 21.

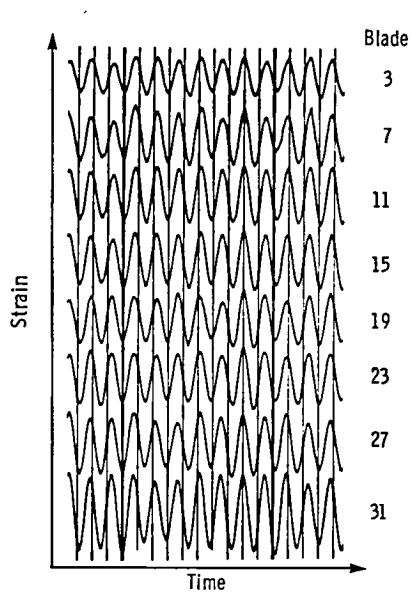

Figure 12. – Raw strain-gage signals for umbrella mode. Rotational speed, 10 000 rpm; shroud gages.

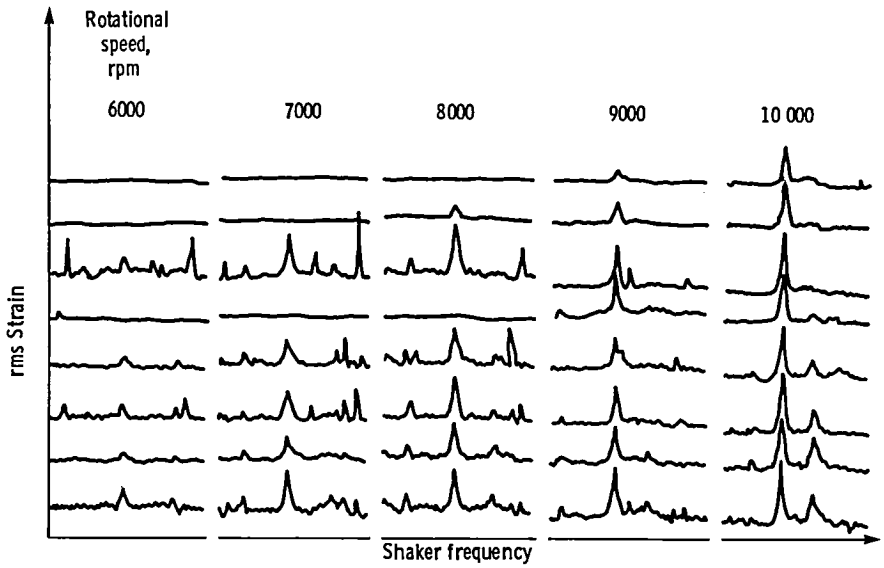

Figure 13. – Root-mean-square shroud gage records showing lockup. C gages; runs 98 to 102.

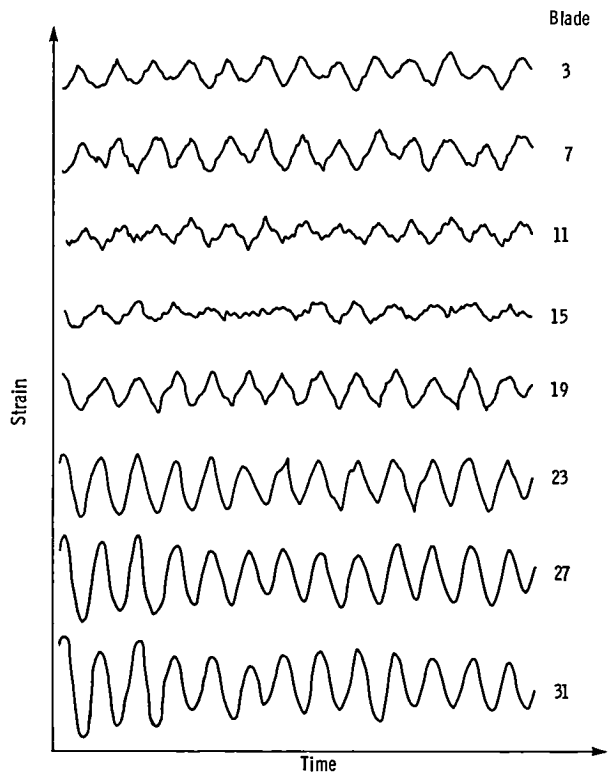

Figure 14. – Raw strain-gage signals for one-nodal-diameter first bending mode. Rotational speed, 10 000 rpm; C gages; run 102.

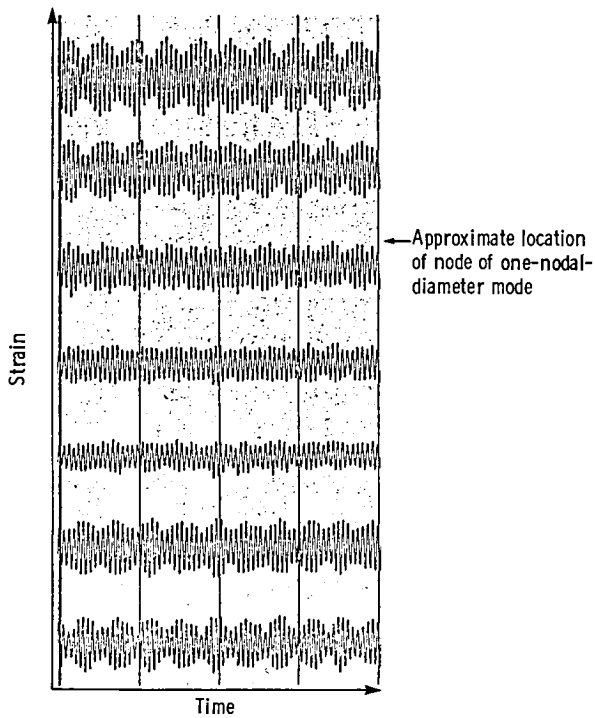

Figure 15. – First bending modes with zero and one nodal diameters, produced simultaneously at 15 000 rpm with shaker operating at 651 Hz. Run 143.

the lower traces because the one-nodal-diameter component has opposite phases in the two regions, whereas the umbrella component has the same phase everywhere.

The observed frequency of the one-nodal-diameter mode at two rotational speeds is shown in figure 9(a). The observed frequencies are slightly higher than the calculated ones. This mode was not easy to excite and identify.

As previously noted the first torsion family of modes is relatively closely spaced around 2000 Hz. The frequencies of the modes in the family as a function of rotational speed, as calculated from the NASTRAN model, are

shown in figure 9(c). It is difficult to excite torsional modes in the rig with clearly identifiable numbers of nodal diameters. The near coincidence of the frequencies of the zero- and one-nodal-diameter modes apparently contributes to this difficulty. Mistuning may also contribute effects due to mode splitting.

Figure 16(a) shows two torsion strain-gage records in which one group of blades exhibits torsion in phase at one frequency (1980 Hz) and a different group resonates at a nearby frequency (2000 Hz). An rms presentation of the response to a frequency sweep through the resonances is shown in figure 16(b). This pair of resonances might be due to a superposition of the closely spaced zero- and one-nodal-diameter modes or to a case of dual modes caused by mistuning. The second possibility has been explored for a mistuned circular disk by other investigators (ref. 3). Further study would be needed with more monitored strain gages and a better signal-to-noise ratio to clarify the situation for rotor 12.

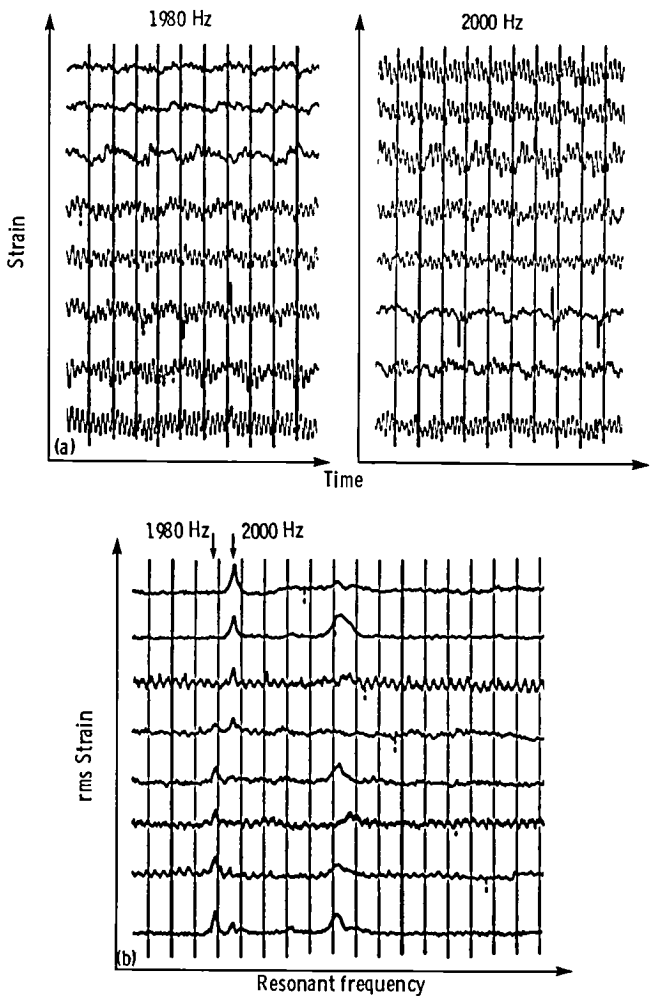

(a) Root-mean-square torsional response showing pair of modes.
(b) Closely spaced pair of torsional modes.

Figure 16. – Torsion strain-gage records. Rotational speed, 12 000 rpm; run 217.

Damping Measurements in the Rig

It is difficult to eliminate damping from the support of a component that is to be vibration tested. Hence any measurement of damping usually has an unknown contribution from the support. This is especially true for certain modes in the spin rig.

Because the rotor is suspended in resilient mounts so that the shakers can vibrate the shaft, those modes that react on the shaft have relatively high damping. In the first bending family such modes include the umbrella mode (which involves a reaction force from the shaft) and the one-nodal-diameter mode (which requires a reaction moment from the shaft). Figure 17 shows the decay of the umbrella mode after the shaker is cut off. As calculated from the decay rate the damping factor ζ associated with the umbrella mode at 12 000 rpm is about 2 percent. The corresponding value for the one-nodal-diameter mode at 10 000 rpm is 1.7 percent. Because modes higher than one nodal diameter do not require shaft reaction, they would be expected to have less damping. However, pure system modes with more than one nodal diameter have not yet been clearly identified in the disk.

At speeds where lockup of the shroud ring is not firm (see fig. 13 and its discussion), modes with very sharp resonance peaks sometimes show up on individual strain-gage signals. Such a mode can be seen in the third trace from the top of figure 13 at 6000 and 7000 rpm and also in figure 18 (third trace from the top). The damping factor for this mode, calculated from the decay rate, is

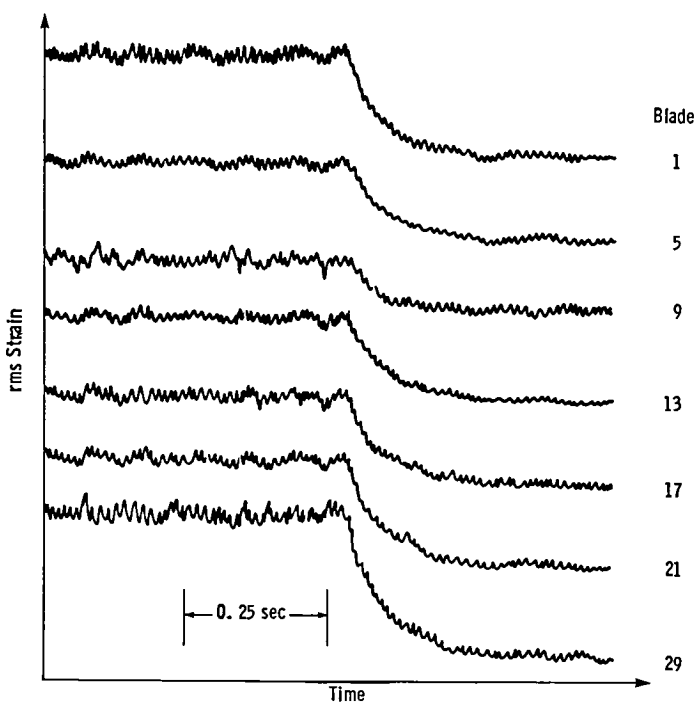

Figure 17. – Decay of umbrella mode at 589 Hz upon shutoff at shakers (rms presentation). Rotational speed, 12 000 rpm; C gages; run 121.

0.13 percent (fig. 19). This value is much lower than those for the system modes discussed previously, probably because of lower reaction on the shaft and hence less dissipation in the resilient shaft suspension. The damping factor for this sharp mode is of the order of values obtained in tests on the two-blade rotor, to be discussed in a later section. It appears that a redesigned rotor support that provides flexibility but does not involve resilient rotor mounts would offer advantages in the form of higher vibration amplitudes and narrower resonances for modes that react on the shaft.

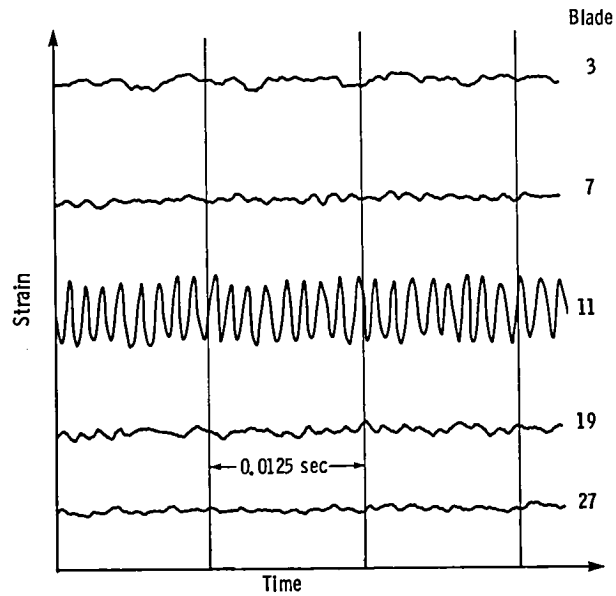

Figure 18. – Mode with very strong response of a single blade below shroud lockup speed. Rotational speed, 7000 rpm; B gages.

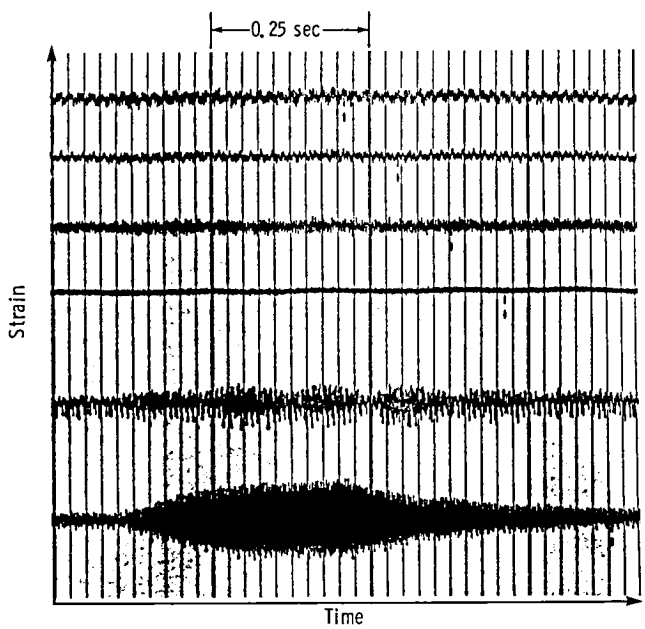

Figure 19. – Growth and decay of localized blade response. Rotational speed, 7000 rpm; B gages.

Air-Jet Excitation

A single air jet was installed in an attempt to excite modes with more than one nodal diameter. Both bending and torsional modes can be produced by the air jet. The modes produced by the jet have not been analyzed completely, but it is clear that the jet is a valuable addition to the excitation methods available. It has been possible to produce many engine-order resonances. Figure 20 shows a set of raw strain-gage records from the B gages (which are sensitive to bending) of the 56-blade rotor as a function of rotational speed with the air jet operating. The same data in the rms presentation are shown in figure 21. A similar set of records from the A gages in the rms presentation is shown in figure 22. The results in figures 20 to 22 show that many resonances occur but that in most cases not all of the blades resonate at the same rotational speed. In a perfectly tuned bladed disk one would expect the air jet to excite modes with nodes that are stationary in the laboratory reference frame rather than in the rotating frame of the disk (which

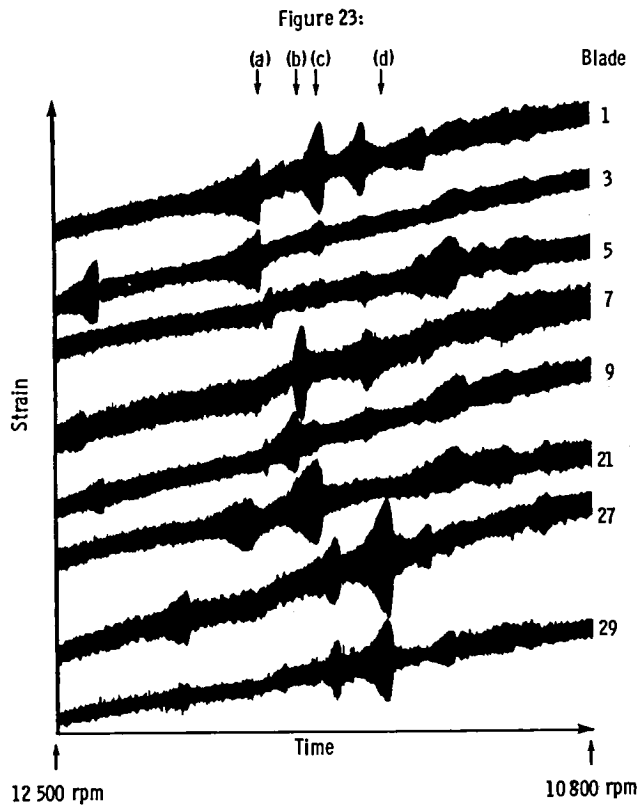

Figure 20. – Raw strain-gage signals during coastdown with air jet on. B gages; run 288.

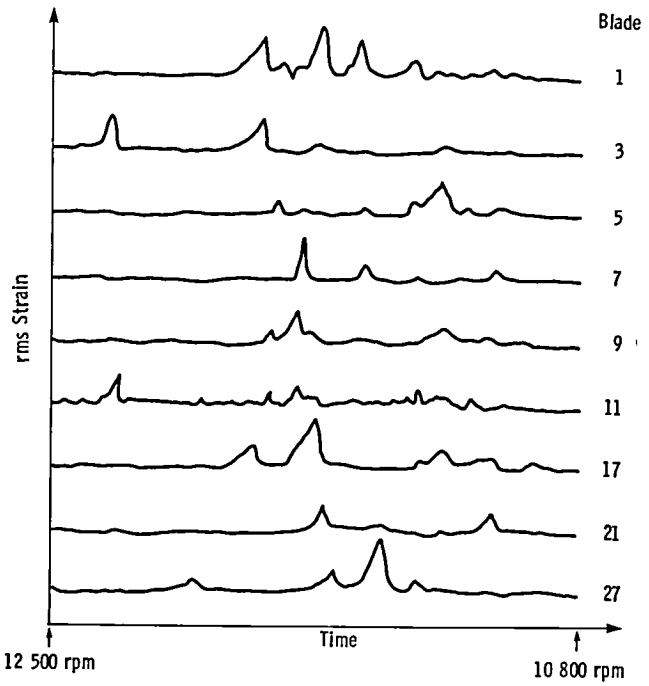

Figure 21. – Root-mean-square record of bending strain-gage signals during coastdown with air jet on. B gages; run 288.

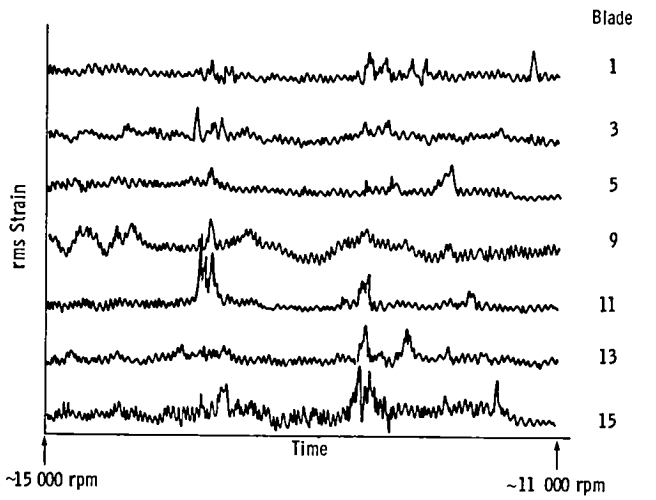

Figure 22. – Root-mean-square record of torsion strain-gage signals during coastdown with air jet on. A gages; run 290.

was the case for shaker excitation). Each blade would therefore perform the same sinusoidal oscillation as every other blade, but with a phase corresponding to its location on the wheel. This should be true for each pure nodal diameter mode. But figure 20 clearly shows vibrational activity of blades at only certain locations on the wheel at any given rotational speed. Mistuning could lead to localized activity of this sort. Figure 23 shows raw strain-gage records corresponding to the rotational speeds indicated by arrows in figure 20.

Experimental Complications with the 56-Blade Rotor

A number of effects complicate the acquisition, from a bladed disk such as rotor 12, of reproducible data that are susceptible to analysis. Some of these effects reflect conditions that can occur in real engine systems to an even greater degree. The most glaring example is the change of the rigidity and continuity of the shroud ring.

Solely mechanical aspects of shroud lockup are one class of effect. In rotor 12 all of the shrouds are designed to be, and appear to be, in at least light contact at zero speed, although sliding of adjacent segments can be produced by hand. The presence of apparent single-blade modes at speeds below about 8000 rpm and the nonuniform response of various blades in the umbrella mode below that approximate speed (fig. 13) suggest that firm lockup exists only above that speed. Thus the character of the modes and the damping is expected to be different above and below that speed.

In addition, differential thermal expansion effects arise in the disk and the shroud ring. These effects were explored qualitatively by observing the rise of the bearing temperatures with time and the variation of the compressive stress in the shrouds as found from the dc component of the signals from the C gages, which are mounted on the shrouds. For a short time after startup, with the shaft, disk, blades, and shrouds at the same temperature, the parts all have known relative dimensions. As the rotor spins at constant speed, however, the bearings heat up, and by conduction through the rotor shaft, the disk begins to heat and to expand. As this occurs, the shroud ring loosens because radial growth of the disk and of the blades increases the diameter of the shroud ring. As time passes, the shroud ring eventually heats up and expands and this retightens the ring. A steady state is never completely reached during a 1- or 2-hr run because the bearings continue to heat.

The heating of the blades also warms the strain gages and changes their sensitivity. The gradual thermal strain of the metal on which the gages are mounted also yields a dc drift of the strain-gage output. For dynamic measurements this dc drift is not too troublesome, except that amplifiers can be saturated by the dc component. Unless the measurement system is ac coupled, intermittent readjustment of the strain-gage bucking voltage is required.

Such problems as these are annoying rather than fundamental difficulties, of course. But in real engines with more extreme and rapidly changing thermal environments, they would be more marked. And some effects, such as the differential expansion of the disk and the shroud ring, can affect both the frequency and damping of the modes.

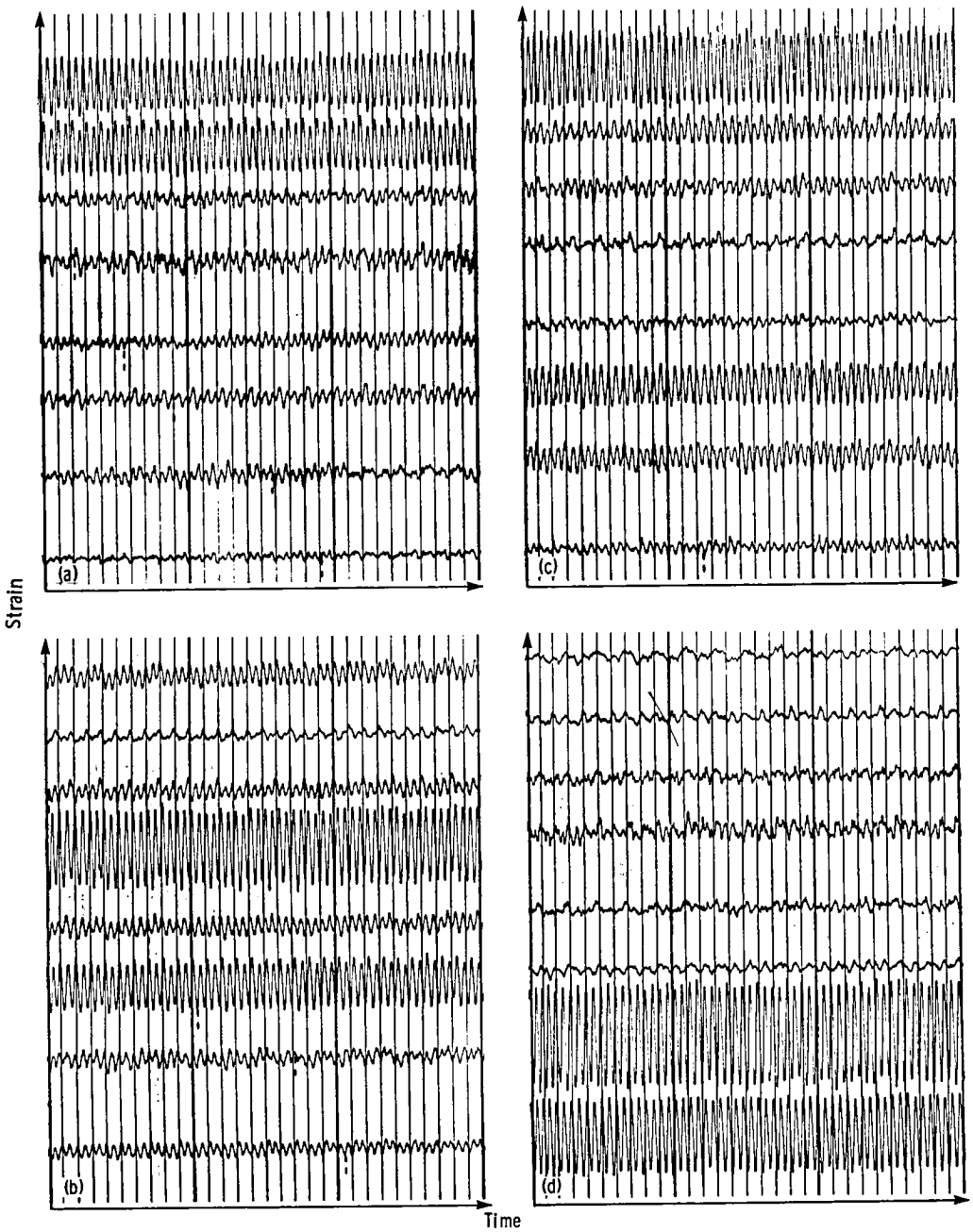

Figure 23. – Raw strain-gage records of modes excited by air jet at rotor speeds indicated by arrows in figure 20.

Two-Blade Rotor Tests

A rotor was constructed to hold two unshrouded blades with simple shapes in order to provide experimental data to check the adequacy of analytical methods of predicting blade frequencies. Kielb, Leissa, and MacBain (see ref. 4 and references therein) defined a series of blades of uniform thickness and uniform twist and various values of aspect ratio and chord-to-thickness ratio. Interested organizations were invited to predict resonant frequencies for these blades for the static (i.e., nonrotating) case. Bench holography was used to measure the frequencies, and the complete static results are reported in reference 4.

The rotor used for obtaining resonant frequencies for the blades when they are rotating is shown in figure 24; flat-plate steel blades with an aspect ratio of 3 and a chord-to-thickness ratio of 20 were mounted on the rotor. The fixture was constructed to allow setting angles of 0°, 30°, 60°, and 90° (measured between the blade plane at the root, in the unswept configuration, and the axis of rotation) and sweep angles of 0°, 22.5°, and 45°

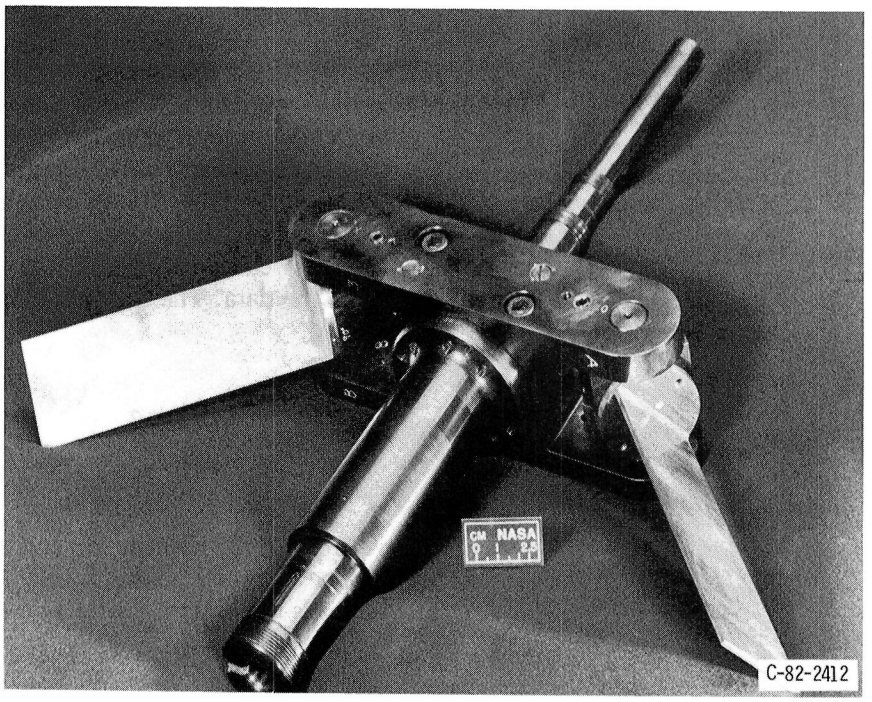

Figure 24. – Two-blade rotor with adjustable sweep and setting angles.

(measured between the blade centerline and the plane of rotation). Strain gages were mounted on each blade as shown in figure 25. Table I shows the frequencies of the first 12 nonrotating modes of these flat plates predicted by a NASTRAN analysis, the frequencies measured by bench holography, the frequencies measured by a bench test using electromagnetic excitation and microphone sensing, and the frequencies observed in the nonrotating spin rig. The agreement between the bench results and the rig results at zero speed is very good. Modes to about 8000 Hz were easily excited by the shakers.

The rotating resonant frequencies of the first five modes were measured to permit calculation of the Southwell coefficients. The measured frequencies as functions of rotational speed are plotted in figure 26. Both the electromagnetic shakers and the air jet were

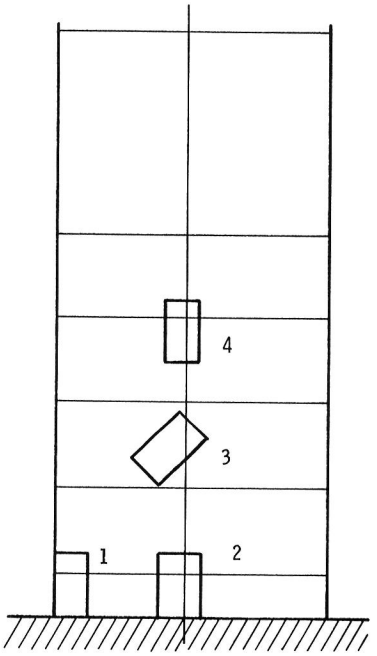

Figure 25. – Strain-gage locations on 15×5×0.25 cm (6×2×0.1 in.) steel flat plates.

TABLE I. – COMPARISON OF CALCULATED AND EXPERIMENTAL STATIC FREQUENCIES

Mode[a]	NASTRAN[b]	Holography	Bench tests	Static spin rig
		Static frequency, Hz		
1B	94.2	93.0	94.2	94.2
1T	575	572	573	572
2B	588	586	586	586
3B	1649	1628	1638	1632,1655
2T	1806	1793	1795	1795
4B	3234	3229	3200	3209
3T	3262	3249	3238	3258
4T	5054	5019	5009	5013
1P	5249	(c)	5312	5313
2P	5563	5593	5592	5595
3P	6348	(c)	6402	6401
5T	7263	7177	7206	7178
4P	7843	7866-7897	7880	-------

[a]B denotes bending, T denotes torsion, P denotes plate modes.

[b]Normalized to give the experimentally observed first bending frequency.

[c]Not observed.

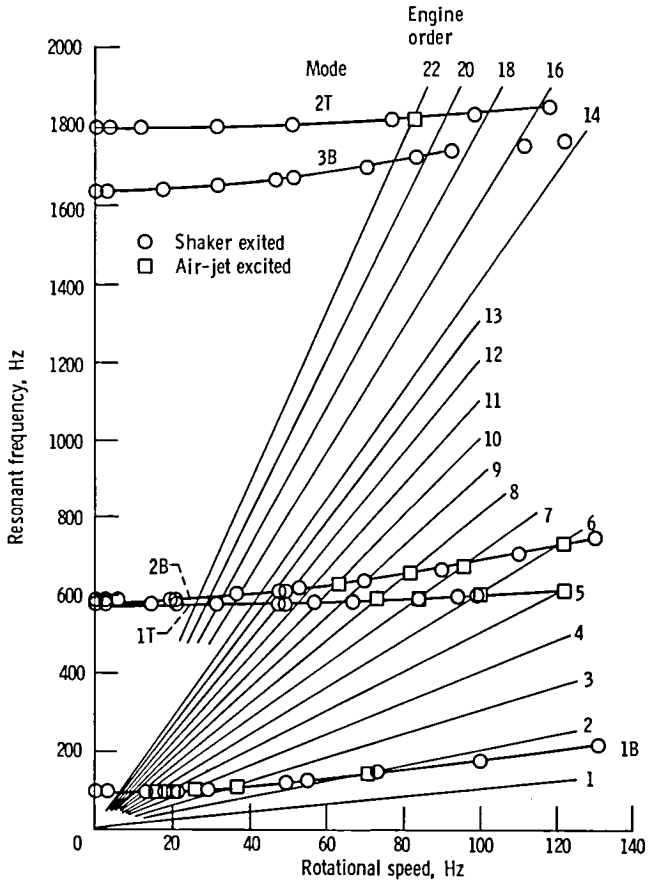

Figure 26. – Campbell diagram for 15×5×0.25 cm (6×2×0.1 in.) steel flat plate.

TABLE II. – RESONANCES EXCITED BY AIR JET IN TWO-BLADE ROTOR

Mode[a]	Engine order[b]	Rotational speed, Hz	Observed frequency,[c] Hz
1B	2	71	142
	3	37	111
	4	26	104
	5	20	100
	6	16	96
1T	5	122	610
	6	100	600
	7	84.5	592
	8	73.5	588
2B	6	122	732
	7	96	672
	8	82	656
	10	63	630
2T	22	83.5	1840

[a]B denotes bending; T denotes torsion.

[b]Obtained by comparing strain-gage output and engine one-per-revolution signals on dual-trace oscilloscope.

[c]Rotational speed times engine order.

used to excite the vibrations. Some of the resonances excited by the air jet are tabulated in table II and plotted in figure 26. The air jet results agree well with the shaker results. The precision of the values of resonant frequency is good because of relatively low damping in the fixture. The half-power widths of the first five modes are tabulated in table III, as well as the damping factors derived from the half-power widths.

Southwell coefficients for the five modes were derived from the data. The Southwell coefficients S are defined by

$$\left(\frac{\omega}{\omega_o}\right)^2 = 1 + S\left(\frac{\Omega}{\omega_o}\right)^2 \tag{1}$$

where ω_o is the nonrotating angular frequency of a given mode, Ω is the rotating angular frequency of the rotor, and ω is the observed rotating resonant frequency of the

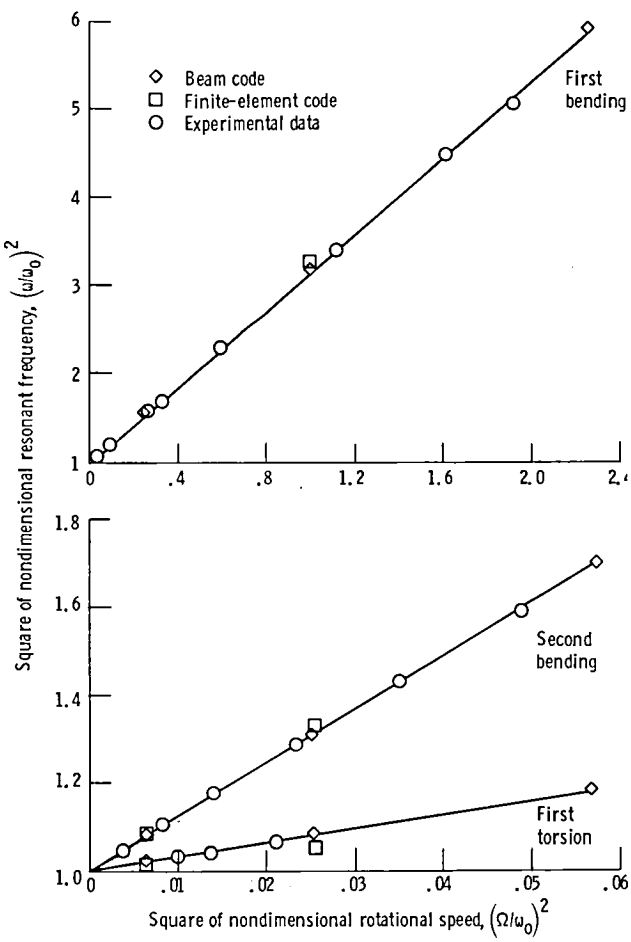

Figure 27. – Quadratic plot of resonant frequency as a function of rotational speed for first and second bending and first torsion modes for 15×5×0.25 cm (6×2×0.1 in.) steel flat plate. Southwell formula: $(\omega/\omega_o)^2 = 1 + S(\Omega/\omega_o)^2$.

blade, all in radians per second. Plots of the left side of equation (1) as a function of the quadratic variable on the right are presented in figures 27 and 28 for the first three bending modes and the first two torsion modes. The precision with which the data, except for the third bending mode, conform to the form of equation (1) is remarkable and gratifying. The third bending mode has a double peak and will require further investigation. The rotating frequencies predicted by a beam method (ref. 5) and by a finite-element code (MacNeal Schwendler/NASTRAN) are also plotted in figures 27 and 28 and are tabulated in table III along with the experimentally derived results.

The ease of producing and observing the modes and the good agreement of the rig results with bench results leads one to expect that the rig results for the other setting and sweep angles and for flat and twisted blades will provide reliable checks for analytical predictions.

TABLE III.–SOUTHWELL COEFFICIENTS FOR 15×5×0.25 cm (6×2×0.1 in.) FLAT PLATE

[Blade in plane of rotation; root 10 cm (4 in.) from axis of rotation.]

Mode	Observed frequency in rig, Hz	Southwell coefficient			Half-power width, $\Delta f/f$	Damping factor, ζ, percent critical
		Experimental	Calculated			
			Beam	Finite element		
1B	94.5	2.16±0.03	2.21±0.02	2.18	0.0032	0.16
1T	573	3.15±0.1	3.25±0.06	2.93	.00083	.041
2B	587	12.3±0.1	12.2±0.01	11.9	.0013	.065
3B	[a]1640	[b]30,42	34.40±0.07	32.1	[b].0071	.35
2T	1796	13.9±0.1	14.8±0.6	13.7	.00089	.044

[a]Average of two observed frequencies.
[b]Double peak.

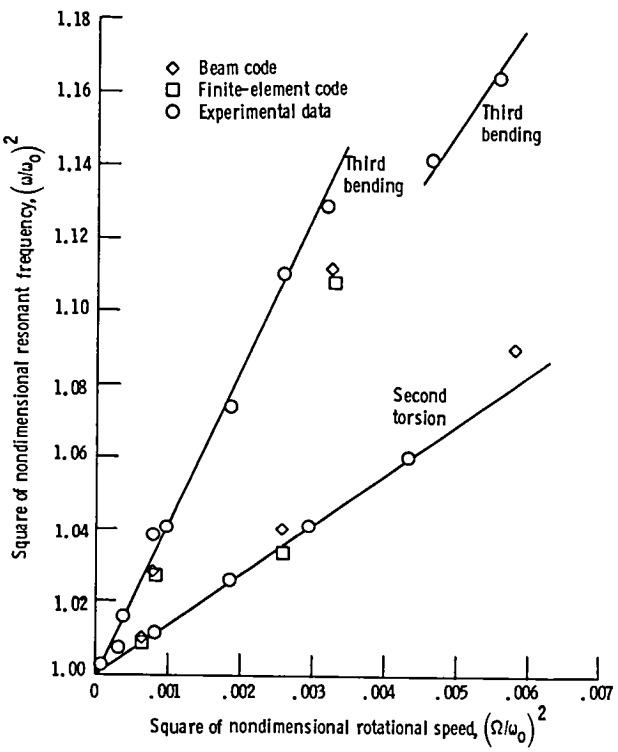

Figure 28.—Quadratic plot of resonant frequency as a function of rotational speed for third bending and second torsion modes for 15×5×0.25 cm (6×2×0.1 in.) steel flat plate.

Concluding Remarks

The results obtained from the experiments on the two-blade rotor show that high-precision vibration information can be obtained from the Lewis spin rig. Factors contributing to this precision include steady speed control and low damping in the two-blade rotor. Bending, torsion, and plate modes with frequencies to about 8000 Hz can be produced that approach bench-test data frequencies as the rotational speed approaches zero. The data from the two-blade rotor for various sweep and setting angles, to be reported elsewhere, have more than adequate precision to check analytical methods for vibration of blades in and out of the plane of rotation.

The analysis made so far of the available data for the 56-blade rotor does not make clear whether some aspects of the system vibration of a multiblade system will be easily extracted from the rig. Modes with two or more nodal diameters have not been produced in a pure form, and methods of decomposing some of the more complex motions produced (especially by the air jet) have not yet been vigorously pursued. Furthermore no attempt to analyze frequencies above about 2300 Hz has been made. However, the excellent results obtained from the two-blade rotor imply that the rig is a reasonably high-precision instrument. Some modifications are considered desirable, such as reducing the damping in the rotor support system. Such minor mechanical improvements, thorough bench tests prior to spinning, the use of the optical blade-tip observation system, and the decomposition of complex modes (such as those produced by the air jet) should permit the high precision obtained with the two-blade rotor to be approached in the analysis of multiblade rotors.

Lewis Research Center
National Aeronautics and Space Administration
Cleveland, Ohio, December 30, 1983

References

1. Frarey, J. L.; Petersen, N. J.; and Hess, D. A.: Turbojet Blade Vibration Data Acquisition Design and Feasibility Testing. (SRC-TR-78-36, Shaker Research Corp.; NASA Contract NAS3-21015.) NASA CR-159505, 1978.
2. Moore, R. D.; and Reid, L.: Performance of a Single-Stage Axial-Flow, Transonic Compressor Stage with a Blade Tip Solidity of 1.7. NASA TM X-2658, 1972.
3. Stange, W. Q.; and MacBain, J. C.: An Investigation of Dual Mode Phenomena in a Mistuned Bladed-Disk. ASME Paper 81-DET-133, Sept. 1981.
4. Leissa, A. W.; MacBain, J. C.; and Kielb, R. E.: Vibrations of Twisted Cantilevered Plates—A Summary of Previous and Current Studies. J. Sound Vibr., vol. 96, no. 1, Sept. 8, 1984.
5. Kaza, K. R. V.; and Kielb, R. E.: Coupled Bending-Bending-Torsion Flutter of a Mistuned Cascade with Nonuniform Blades. NASA TM-82813, 1982.

1. Report No.	2. Government Accession No.	3. Recipient's Catalog No.
NASA TP-2304		

4. Title and Subtitle	5. Report Date
Lewis Research Center Spin Rig and Its Use in Vibration Analysis of Rotating Systems	May 1984
	6. Performing Organization Code: 505-33-52

7. Author(s)	8. Performing Organization Report No.
Gerald V. Brown, Robert E. Kielb, Erwin H. Meyn, Richard E. Morris, and Stephen J. Posta	E-1829
	10. Work Unit No.

9. Performing Organization Name and Address	11. Contract or Grant No.
National Aeronautics and Space Administration Lewis Research Center Cleveland, Ohio 44135	
	13. Type of Report and Period Covered: Technical Paper

12. Sponsoring Agency Name and Address	14. Sponsoring Agency Code
National Aeronautics and Space Administration Washington, D.C. 20546	

15. Supplementary Notes

16. Abstract

The Lewis Research Center spin rig was constructed to provide experimental evaluation of analysis methods developed under the NASA Engine Structural Dynamics Program. Rotors up to 51 cm (20 in.) in diameter can be spun to 16 000 rpm in vacuum by an air motor. Vibration forcing functions are provided by shakers that apply oscillatory axial forces or transverse moments to the shaft, by a natural whirling of the shaft, and by an air jet. Blade vibration is detected by strain gages and optical blade-tip motion sensors. A variety of analog and digital processing equipment is used to display and analyze the signals. Results obtained from two rotors are discussed. A 56-blade compressor disk was used to check proper operation of the entire spin rig system. A special two-blade rotor was designed and used to hold flat and twisted plates at various setting and sweep angles. Accurate Southwell coefficients have been obtained for several modes of a flat plate oriented parallel to the plane of rotation.

17. Key Words (Suggested by Author(s))	18. Distribution Statement
Structural dynamics; Bladed-disk vibration; Spin rig; Turbine engine; Vibration measurement; Turbomachinery vibration	Unclassified - unlimited STAR Category 07

19. Security Classif. (of this report)	20. Security Classif. (of this page)	21. No. of pages	22. Price*
Unclassified	Unclassified	18	A02

*For sale by the National Technical Information Service, Springfield, Virginia 22161

NASA-Langley, 1984

National Aeronautics and
Space Administration

Washington, D.C.
20546

Official Business
Penalty for Private Use, $300

THIRD-CLASS BULK RATE

Postage and Fees Paid
National Aeronautics and
Space Administration
NASA-451

NASA

POSTMASTER: If Undeliverable (Section 158 Postal Manual) Do Not Return